Article

Nonstationary Analyses of the Maximum and Minimum Streamflow in Tamsui River Basin, Taiwan

Jenq-Tzong Shiau * and **Yi-Ting Liu**

Department of Hydraulic and Ocean Engineering, National Cheng Kung University, Tainan 701, Taiwan; toka122400@gmail.com

* Correspondence: jtshiau@mail.ncku.edu.tw; Tel.: +886-6-2757575 (ext. 63242)

Abstract: This study aims to detect non-stationarity of the maximum and minimum streamflow regime in Tamsui River basin, northern Taiwan. Seven streamflow gauge stations, with at least 27-year daily records, are used to characterize annual maximum 1- and 2-day flows and annual minimum 1-, 7-, and 30-day flows. The generalized additive models for location, scale, and shape (GAMLSS) are used to dynamically detect evolution of probability distributions of the maximum and minimum flow indices with time. Results of time-covariate models indicate that stationarity is only noted in the 4 maximum flow indices out of 35 indices. This phenomenon indicates that the minimum flow indices are vulnerable to changing environments. A 16-category distributional-change scheme is employed to classify distributional changes of flow indices. A probabilistic distribution with complex variations of mean and variance is prevalent in the Tamsui River basin since approximate one third of flow indices (34.3%) belong to this category. To evaluate impacts of dams on streamflow regime, a dimensionless index called the reservoir index (RI) serves as an alternative covariate to model nonstationary probability distribution. Results of RI-covariate models indicate that 7 out of 15 flow indices are independent of RI and 80% of the best-fitted RI-covariate models are generally worse than the time-covariate models. This fact reveals that the dam is not the only factor in altering the streamflow regime in the Tamsui River, which is a significant alteration, especially the minimum flow indices. The obtained distributional changes of flow indices clearly indicate changes in probability distributions with time. Non-stationarity in the Tamsui River is induced by climate change and complex anthropogenic interferences.

Keywords: non-stationarity; streamflow regime; annual flow index; reservoir index; GAMLSS

1. Introduction

Probabilistic theories have played an essential role in hydraulic facilities planning and design due to the inherent uncertainties involved in hydro-climatic series. It has become a standard practice to employ frequency analysis of extreme hydro-climatic variables in the risk evaluation of hydraulic facilities [1,2]. An important assumption in such frequency analysis-based approaches is stationarity; that is, the probability distribution used to fit the variable of interest is time invariant. However, climate change and/or anthropogenic interference-induced changing environments may lead to alterations in statistical characteristics of hydro-climatic variables, and thus, result in non-stationarity. Non-stationarity in hydro-climate series renders estimates of return period and risk used for hydraulic facilities planning and design ambiguous and questionable [3–7].

Recent studies [8–17] have showed strong evidence of climate change impacts on the rainfall regime. Alterations in rainfall regime propagate through the hydrologic cycle, and thus induce changing streamflow regime. Impacts of climate change and anthropogenic activities on streamflow regime have drawn considerable attention recently [18–23]. A vast literature has thus been devoted to exploring non-stationarity in streamflow series worldwide [24–31]. However, most studies focus on extreme streamflow such as flood or low flow, while few studies have investigated them simultaneously.

Focusing on Taiwan, evidence of altering rainfall regime induced by climate change was indicated by several recent studies [32–38]. However, little research has examined the changes in streamflow regime in Taiwan, with the exception of Yeh et al. [39] who investigated the long-term streamflow trend in northern Taiwan using the Mann-Kendall test. Nonstationary modeling of streamflow in Taiwan is rarely addressed in the literature.

The main aim of this work is to detect the presence of non-stationarity in the streamflow regime, characterized by the maximum and minimum flow indices at various time scales, of the Tamsui River located in northern Taiwan. The generalized additive models for location, scale, and shape (GAMLSS), developed by Rigby and Stasinopoulos [40], are adopted for detecting non-stationarity in streamflow characteristics by respectively incorporating time-dependent parameters and anthropogenic-impact parameters in terms of reservoir index into probability models. In addition, the 16-category distributional-change scheme, proposed by Shiau and Wu [41], is also used to classify variations of the obtained nonstationary distributions of the flow indices for distinguishing spatial variability. The obtained information may usefully guide future planning and design of water-resources engineering, adapting to the changing environment.

2. Methodology

2.1. The Generalized Additive Models for Location, Scale, and Shape (GAMLSS)

A widely used approach to model nonstationary hydro-climatic series is the time-varying moments method, indicated by Khaleq et al. [42], which incorporates time-varying parameters into probability models with the same form of stationary condition. The GAMLSS is a popular tool to achieve this purpose in hydrology and dynamically detects evolution of probability distributions with time or other covariates [43–46].

In GAMLSS, the independent observations y_i ($i = 1, 2, \ldots, n$) are assumed to have a probability density function (PDF) $f(y_i | \theta^i)$, where $\theta^i = \left(\theta_1^i, \ldots, \theta_p^i \right)$ is a parametric vector accounting for location, scale, and shape. p denotes the number of parameters and is usually less than or equal to four. The distribution parameters are related to the explanatory variables (covariates) by the monotonic link functions g_k ($k = 1, \ldots, p$), which is expressed as

$$g_k(\theta_k) = \mathbf{X}_k \boldsymbol{\beta}_k + \sum_{j=1}^{m} h_{jk} \tag{1}$$

where g_k denotes the monotonic link function for the kth parameter (here only the identity and logarithm link functions are considered); $\mathbf{X}_k$ represents an $n \times m$ matrix of explanatory variables (covariates); $\boldsymbol{\beta}_k^T = (\boldsymbol{\beta}_{1k}, \boldsymbol{\beta}_{2k}, \ldots, \boldsymbol{\beta}_{mk})$ is a parameter vector of length m; and h_{jk} represents the functional dependence of the distribution parameters on explanatory variables x_{jk}.

In this study, a semi-parametric additive formulation is adopted to model non-stationarity in flow indices in the Tamsui River basin, Taiwan; that is, functional dependence is linear or smooth and smooth dependence is based on the cubic spline function in this study. Further details of GAMLSS can be found in Rigby and Stasinopoulos [40].

A total of five widely used two-parameter distributions, including lognormal (LNO), logistic (LO), gamma (GA), Gumbel (GU), and Weibull (WEI), are employed to model the flow indices. The PDFs associated with types of link function of these distributions are summarized in Table 1. The mean and variance of these distributions in terms of parameters (θ_1 and θ_2) are reported in Table 2. The parameters of the probability distributions are modeled as functions of the time or reservoir index, which is described in the subsequent subsection. To avoid model over-fitting, the minimum Akaike Information Criterion (AIC) is adopted in this study to select a parsimonious model. Calculations are implemented by a free-access R-based package gamlss [47].

Table 1. Summaries of probability density function (PDF) of five distributions and the link functions used to model flow indices.

Distribution	Probability Density Function	Range of Parameters	Types of Link Function	
			θ_1	θ_2
Lognormal (LNO)	$f(y) = \frac{1}{\sqrt{2\pi}\theta_2 y} exp\left[-\frac{(\log y - \theta_1)^2}{2\theta_2^2}\right], \quad y > 0$	$\theta_1 > 0, \theta_2 > 0$	identity()	ln()
Logistic (LO)	$f(y) = \frac{\exp\left(-\frac{y-\theta_1}{\theta_2}\right)}{\theta_2\left[1+\exp\left(-\frac{y-\theta_1}{\theta_2}\right)\right]^2}, \quad -\infty < y < \infty$	$-\infty < \theta_1 < \infty, \theta_2 > 0$	identity()	ln()
Gamma (GA)	$f(y) = \frac{1}{\left(\theta_2^2\theta_1\right)^{1/\theta_2^2}}\frac{y^{\frac{1}{\theta_2^2}-1}\exp\left(-\frac{y}{\theta_2^2\theta_1}\right)}{\Gamma\left(1/\theta_2^2\right)}, \quad y > 0$	$\theta_1 > 0, \theta_2 > 0$	ln()	ln()
Gumbel (GU)	$f(y) = \frac{1}{\theta_2}exp\left[\frac{y-\theta_1}{\theta_2} - \exp\left(\frac{y-\theta_1}{\theta_2}\right)\right], \quad -\infty < y < \infty$	$-\infty < \theta_1 < \infty, \theta_2 > 0$	identity()	ln()
Weibull (WEI)	$f(y) = \frac{\theta_2 y^{\theta_2 - 1}}{\theta_1^{\theta_2}}exp\left[-\left(\frac{y}{\theta_1}\right)^{\theta_2}\right], \quad y > 0$	$\theta_1 > 0, \theta_2 > 0$	identity()	ln()

Table 2. Summaries of mean and variance of five distributions in terms of distribution parameters.

Distribution	Mean	Variance	Note
Lognormal (LNO)	$E(Y) = \omega^{1/2}e^{\theta_1}$	$Var(Y) = \omega(\omega - 1)e^{2\theta_1}$	$\omega = \exp\left(\theta_2^2\right)$
Logistic (LO)	$E(Y) = \theta_1$	$Var(Y) = \frac{\pi^2\theta_2^2}{3}$	
Gamma (GA)	$E(Y) = \theta_1$	$Var(Y) = \theta_2^2\theta_1^2$	
Gumbel (GU)	$E(Y) = \theta_1 + 0.57722\theta_2$	$Var(Y) = \frac{\pi^2\theta_2^2}{6}$	
Weibull (WEI)	$E(Y) = \theta_1\Gamma\left(\frac{1}{\theta_2} + 1\right)$	$Var(Y) = \theta_1^2\left\{\Gamma\left(\frac{2}{\theta_2} + 1\right) - \left[\Gamma\left(\frac{1}{\theta_2} + 1\right)\right]^2\right\}$	

2.2. Reservoir Index

To evaluate impacts of dams on the streamflow regime, a dimensionless index called the reservoir index or check dam index has been proposed in the literature [24,48–50]. The dimensionless reservoir index developed by Jiang et al. [50] is adopted in this study to serve as an alternative covariate of nonstationary probabilistic models, which is defined as

$$RI = \sum_{i=1}^{N}\left(\frac{A_i}{A_T}\right)\left(\frac{V_i}{V_T}\right) \tag{2}$$

where N denotes the number of dams upstream of the streamflow gauge station; A_i denotes the catchment area of each reservoir; A_T denotes the catchment area of the gauge station; V_i denotes the capacity of each reservoir; and V_T denotes the total capacity of all dams upstream of the gauge station.

3. Data Used

3.1. Overview of the Tamsui River Basin

Tamsui River, located in northern Taiwan, has a total length of 159 km and a catchment area of 2726 km^2. Originating in Pintain Mountain, the Dahan River (main tributary) wanders northward and northwestward and receives streamflow from the Xindian River and the Jilong River before emptying into the Taiwan Strait (Figure 1). The Tamsui River, flowing through dense population areas in northern Taiwan (Taipei City and New Taipei City), led to the construction of hydraulic facilities, initiated in the early twentieth century. Currently there are 12 dams within this basin offering domestic water-supply, flood-

mitigation, and hydropower-generation purposes. Figure 1 shows the spatial locations of these 12 dams and seven selected streamflow gauge stations to reflect natural and dam-altered sites. Figure 2 shows the schematic layout of the Tamsui River system including tributaries, streamflow gauge stations, and dams, which clearly demonstrates the upstream and downstream locations of dams and stations.
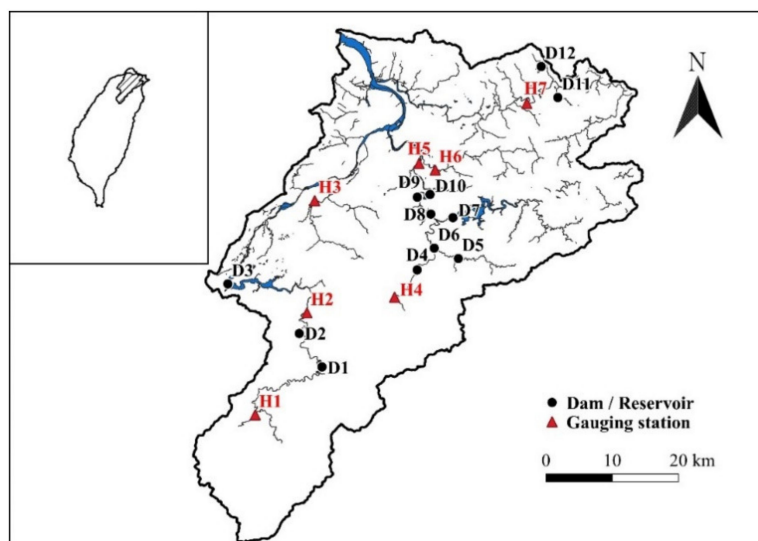

Figure 1. Spatial locations of selected seven streamflow gauge stations (H1 to H7) and 12 dams (D1 to D12) in the Tamsui River basin, Taiwan.
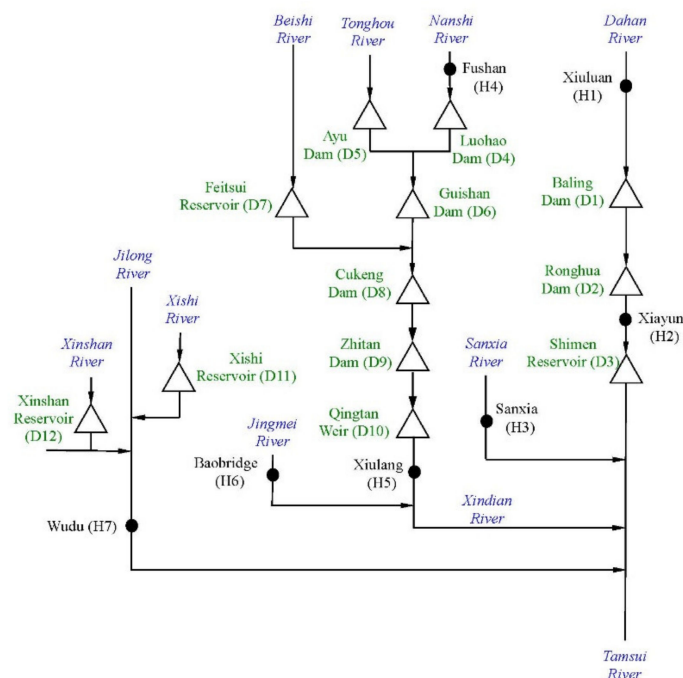

Figure 2. Schematic layout of the Tamsui River system including tributaries, streamflow gauge stations, and dams (not to scale).

According to Shiau and Wu [41], the mean annual total rainfall at Taipei station, with the longest records in the Tamsui River basin, is 2169 mm for the period 1897−2017. Greater temporal variations are noted in the total annual rainfall series at Taipei station. For example, the maximum total annual rainfall is 4392 mm (1992) and the minimum is

1184 mm (2003). The mean and variance of total annual rainfall at Taipei station exhibit an increasing trend [41]. The altered rainfall regime at the Taipei station located in the Tamsui River basin is associated with complex anthropogenic interferences such as urban development and hydraulic-facility operation, leading to changes in streamflow regime.

3.2. Streamflow Data

Basic information on the seven selected streamflow gauge stations in the Tamsui River basin are summarized in Table 3. The daily streamflow of these stations, measured by the Water Resources Agency (Taiwan), are used to evaluate potential streamflow regime alterations within this basin. Due to the fact that parts of the streamflow data are unavailable (missing or unrecorded), the daily streamflow records are not continuous. At least 27-year daily streamflow records are used in this study. The longest streamflow data for 61 years are recorded at H4. It is worth noting that most stations have streamflow records for recent years (after 2014) except that H5 ends its records in 2000.

Table 3. Basic information of seven selected streamflow gauge stations in Tamsui River basin, Taiwan.

Code	Station Name	Station Number	Catchment Area (km^2)	Record Years	Data Length (Years)
H1	Xiuluan	1140H041	115.93	1957–2002, 2009–2011, 2013–2014	51
H2	Xiayun	1140H054	622.80	1963–2002, 2010–2015	46
H3	Sanxia	1140H048	125.34	1957–2002, 2015–2018	49
H4	Fushan	1140H010	160.40	1953–2003, 2005–2008, 2010–2015	61
H5	Xiulang	1140H066	750.76	1970–1971, 1973–2000	32
H6	Baobridge	1140H082	109.22	1987–2002, 2008–2018	27
H7	Wudu	1140H058	204.41	1963–1964, 1966–1999, 2005–2013, 2017–2018	47

The streamflow regime is characterized by the annual maximum and minimum flow indices with various time scales, which include the annual maximum 1-day and 2-day flow (denoted as 1DMAX and 2DMAX) and the annual minimum 1-day, 7-day, and 30-day flow (denoted as 1DMIN, 7DMIN, and 30DMIN), since these annual flow indices evidently relate to flooding and water-supply problems in Taiwan. The annual mean and standard deviation of these flow indices for all selected stations are reported in Table 4. Among these stations, three stations (H2, H5, and H7) have upstream dams that potentially affect the streamflow regime, while the remaining four stations are free of dam impacts.

3.3. Reservoir Index

Basic information on 12 dams located within the Tamsui River basin, including dam height, capacity, catchment area, and finished year, are reported in Table 5. The dam-affected stations (H2, H5, and H7) have different impacts due to the various numbers of upstream dams. Streamflow regime at H2 is influenced by D1 and D2. Streamflow regime at H5 is affected by D4, D5, D6, D7, D8, D9, and D10. Streamflow regime at H7 is influenced by D11 and D12. Figure 3 illustrates the time evolution of RIs, defined by equation (2), of these three stations within the streamflow records. It is worth noting that D1 was removed in 2007 due to dam failure. Evident high-impact RIs are observed at H2 and H5 since the

maximum RI exceeds the threshold of 0.25, which is suggested by López and Francés [48]. Low-impact RI noted at H7 is attributed to smaller catchment areas.

Table 4. Annual mean and standard deviation of the maximum and minimum flow indices for the selected stations in Tamsui River basin, Taiwan.

Code	1DMAX		2DMAX		1DMIN		7DMIN		30DMIN	
	Mean (m³/s)	STD (m³/s)	Mean (m³/s)	STD (m³/s)	Mean (m³/s)	STD (m³/s)	Mean (m³/s)	STD (m³/s)	Mean (m³/s)	STD (m³/s)
H1	202.7	253.9	138.8	157.9	0.80	0.32	0.85	0.33	1.04	0.37
H2	1201.4	1092.5	845.5	747.4	6.07	4.79	7.27	4.48	8.72	4.99
H3	230.9	169.0	161.1	114.7	0.74	0.43	0.97	0.50	1.58	0.66
H4	378.8	255.5	279.0	174.1	4.20	1.20	4.53	1.27	5.54	1.52
H5	1366.6	829.6	972.7	535.1	3.34	4.16	4.92	5.76	9.10	9.44
H6	234.5	134.8	171.9	92.2	0.75	0.49	0.94	0.49	1.66	0.79
H7	428.5	208.6	334.1	187.3	0.56	0.47	0.69	0.54	1.55	1.05

Table 5. Basic information on dams in Tamsui River basin, Taiwan.

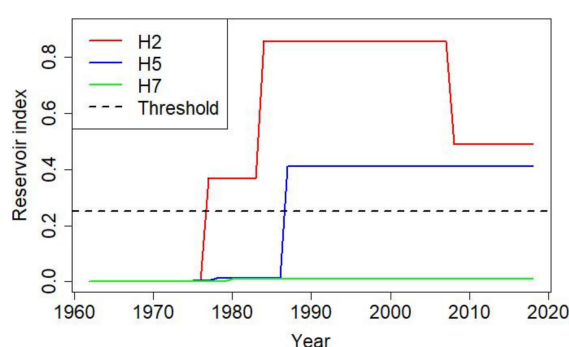| Code	Dams	Dam Height (m)	Total Capacity (×10⁴ m³)	Catchment Area (km²)	Finished Year
D1	Baling Dam	38.0	1047	499.5	1977
D2	Ronghua Dam	82.0	1240	561.6	1984
D3	Shimen Reservoir	133.1	39120	763.4	1964
D4	Luohao Dam	16.0	30.8	210.0	1954
D5	Ayu Dam	9.5	10.5	72.8	1947
D6	GuiShan Dam	10.0	42.3	312.7	1941
D7	Feitsui Reservoir	122.5	40600	303.0	1987
D8	CuKeng Dam	3.6	24.0	645.7	1909
D9	Zhitan Dam	40.0	417.7	679.8	1978
D10	Qingtan Weir	3.0	83.2	716.8	1975
D11	Xishi Reservoir	29.6	45.0	6.7	1926
D12	Xinshan Reservoir	66.0	1000	1.6	1980

Figure 3. Evolution of reservoir index with time at H2, H5, and H7 in Tamsui River basin, Taiwan.

4. Results and Discussion

4.1. Time-Covariate Nonstationary Models of the Maximum and Minimum Flow Indices

Table 6 summaries the best-fitted probability distributions and the corresponding parameter types of the maximum and minimum flow indices for all stations in Tamsui River basin. Variations of mean and variance of the obtained distributions are also summarized in Table 6.

Table 6. Results of the generalized additive models for location, scale and shape (GAMLSS) using time as covariate, corresponding mean and variance variations, and the variation category.

Index	Parameter	H1	H2	H3	H4	H5	H6	H7
1DMAX	Dist.	Lognormal (LNO)	Gamma (GA)	LNO	GA	GA	Weibull (WEI)	GA
	θ_1	c	c	c	c	c	c	t
	θ_2	$cs(t)$	c	c	$cs(t)$	$cs(t)$	c	$cs(t)$
	$E(Y)$	nt	c	c	c	c	c	$T\downarrow$
	$VAR(Y)$	nt	c	c	nt	$nt\uparrow$	c	$nt\downarrow$
	Catgry.	XVI	VI	VI	VIII	V	VI	XI
2DMAX	Dist.	LNO	GA	LNO	GA	GA	WEI	LNO
	θ_1	c	c	c	c	c	$cs(t)$	t
	θ_2	$cs(t)$	$cs(t)$	c	$cs(t)$	$cs(t)$	c	$cs(t)$
	$E(Y)$	nt	c	c	c	c	nt	$nt\downarrow$
	$VAR(Y)$	nt	nt	c	nt	$nt\uparrow$	nt	$nt\downarrow$
	Catgry.	XVI	VIII	VI	VIII	V	XVI	XI
1DMIN	Dist.	LO	WEI	WEI	WEI	GA	WEI	GA
	θ_1	$cs(t)$	$cs(t)$	$cs(t)$	$cs(t)$	$cs(t)$	$cs(t)$	$cs(t)$
	θ_2	c	t	$cs(t)$	c	$cs(t)$	c	$cs(t)$
	$E(Y)$	$nt\uparrow$	$nt\uparrow$	nt	nt	nt	nt	$nt\uparrow$
	$VAR(Y)$	c	$nt\uparrow$	$nt\uparrow$	nt	nt	nt	nt
	Catgry.	II	I	XIII	XVI	XVI	XVI	IV
7DMIN	Dist.	LO	GA	WEI	GA	GA	LNO	GA
	θ_1	$cs(t)$	$cs(t)$	$cs(t)$	$cs(t)$	$cs(t)$	$cs(t)$	$cs(t)$
	θ_2	c	$cs(t)$	$cs(t)$	c	$cs(t)$	$cs(t)$	c
	$E(Y)$	$nt\uparrow$	$nt\uparrow$	nt	nt	nt	nt	$nt\uparrow$
	$VAR(Y)$	c	$nt\uparrow$	nt	nt	nt	nt	$nt\uparrow$
	Catgry.	II	I	XVI	XVI	XVI	XVI	I
30DMIN	Dist.	LO	GA	WEI	GA	LNO	GA	GA
	θ_1	$cs(t)$	$cs(t)$	$cs(t)$	$cs(t)$	$cs(t)$	$cs(t)$	c
	θ_2	c	$cs(t)$	c	t	t	$cs(t)$	$cs(t)$
	$E(Y)$	$nt\uparrow$	$nt\uparrow$	$nt\downarrow$	nt	$nt\downarrow$	nt	c
	$VAR(Y)$	c	$nt\uparrow$	$nt\downarrow$	nt	$nt\downarrow$	nt	$nt\downarrow$
	Catgry.	II	I	XI	XVI	XI	XVI	VII

Note: c: constant; t: linearly time varying; $cs(t)$: cubic spline; nt: nonlinearly time varying; ↑: increasing trend; ↓: decreasing trend.

Stationary 1DMAX is observed at H2, H3, and H6 due to their constant distribution parameters. However, different distributional changes (i.e., different time-variation patterns of parameter) of 1DMAX are noted for the other stations. For example, H7 clearly has nonlinearly declined mean and variance, H5 has nonlinearly increasing variance, H1 and H4 have nonlinearly varying variance, and H4 and H5 have constant mean. Figure 4a–d illustrate curves of various quantiles (0.95, 0.75, 0.5, 0.25, and 0.05 from top to bottom) of 1DMAX at H1, H4, H5, and H7, respectively. Evidently different distributional changes are observed in these stations. For instance, H1 illustrates that the range of 1DMAX changes from wider to narrower and then becomes wider due to nonlinear variance. H7 clearly shows a declined range of 1DMAX caused by declined variance.

Stationary 2DMAX is only observed at H3. The time-varying patterns of 2DMAX at the remaining stations are similar to those of 1DMAX with the exception of the nonstationary distribution parameters noted at H2 and H6. For example, a wider range of 2DMAX is observed at H1 in 1957, the narrowest 2DMAX is noted around 1975 and then gradually increases. The distributional change of 2DMAX at H1 is similar to that of 1DMAX shown in Figure 4a. A gradually reducing range of 2DMAX is noted at H7, which is also similar to the distributional change of 1DMAX shown in Figure 4d.

Non-stationarity is dominant in the minimum flow indices since none of these are categorized as stationarity. This phenomenon implies that the minimum flow is vulnerable to changing environments when compared with the results of the maximum flow indices. Figure 5a–d illustrate variations of quantile curves (0.95, 0.75, 0.5, 0.25, and 0.05 from top to bottom) of 1DMIN at H2, H3, H5, and H7, respectively. Different variation patterns are clearly noted in 1DMIN for various stations. For example, H1 (not shown in Figure 5), H2,

and H7 exhibit an increasing trend of mean, while H2 and H3 have an increasing trend of variance. However, these trends, as well as the variation pattern of mean and variance of other stations, are nonlinear variations, except for the constant variance observed at H1.
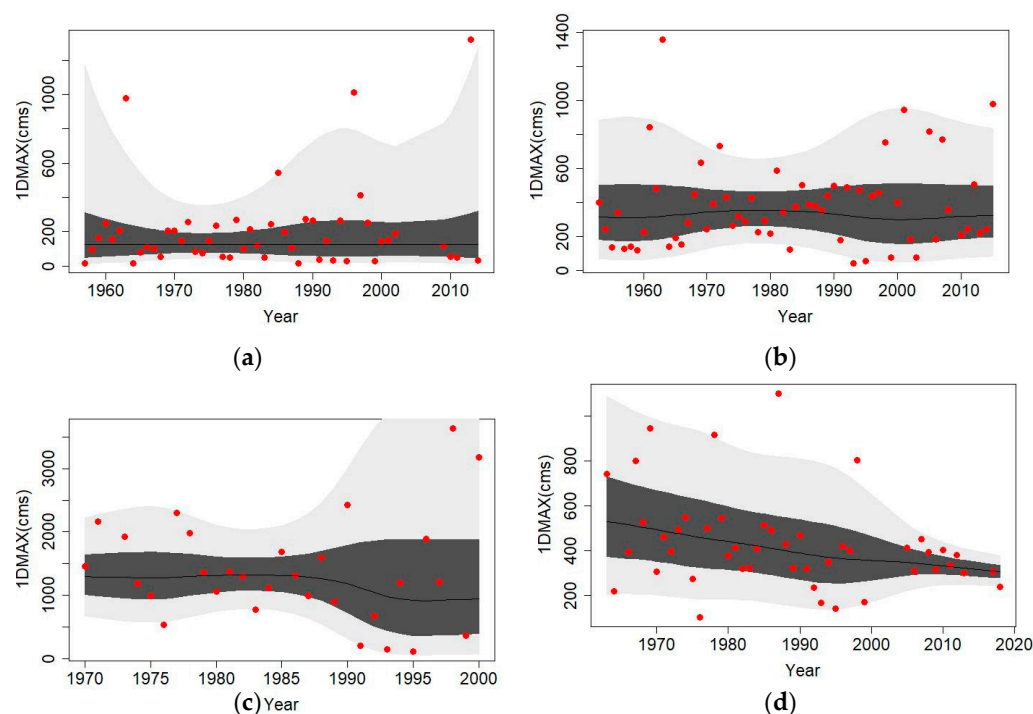

Figure 4. Variations of quantile curves (0.95, 0.75, 0.5, 0.25, and 0.05 from top to bottom) of 1DMAX (annual maximum 1-day streamflow) at (**a**) H1 (Xiuluan), (**b**) H4 (Fushan), (**c**) H5 (Xiulang), and (**d**) H7 (Wudu).

Similar distributional changes between 1DMIN and 7DMIN are observed at most stations. An exception is noted at H7 due to the nonlinear-varying variance of 1DMIN becoming a nonlinearly increasing variance of 7DMIN. Distributional changes of 30DMIN are close to those of 7DMIN at H1, H2, H4, and H6. Significantly decreasing variance of 30DMIN are observed at H3, H5, and H7. In summary, variation patterns among 1DMIN, 7DMIN, and 30DMIN are similar. The most distinct distributional changes among minimum flow indices are that the increasing means of 1DMIN and 7DMIN become a constant mean of 30DMIN, and increasing variance of 7DMIN becomes decreasing variance of 30DMIN at H7.

To gain a consistent description of distributional changes of the maximum and minimum flow indices for various stations, the 16-category distributional-change scheme proposed by Shiau and Wu [41] is adopted in this study. This scheme categorizes distributional changes in terms of variation of mean and variance of probability. Four types of variation in mean and variance (linear or nonlinear increasing, no-change, linear or nonlinear decreasing, and complex variation not belonging to previous types) are adopted in this scheme and lead to 16 categories of distributional change, which are defined in Table 7. Categories of the maximum and minimum inflow indices of all stations are also reported in Table 6. The numbers of indices classified in each category are reported in Table 7.
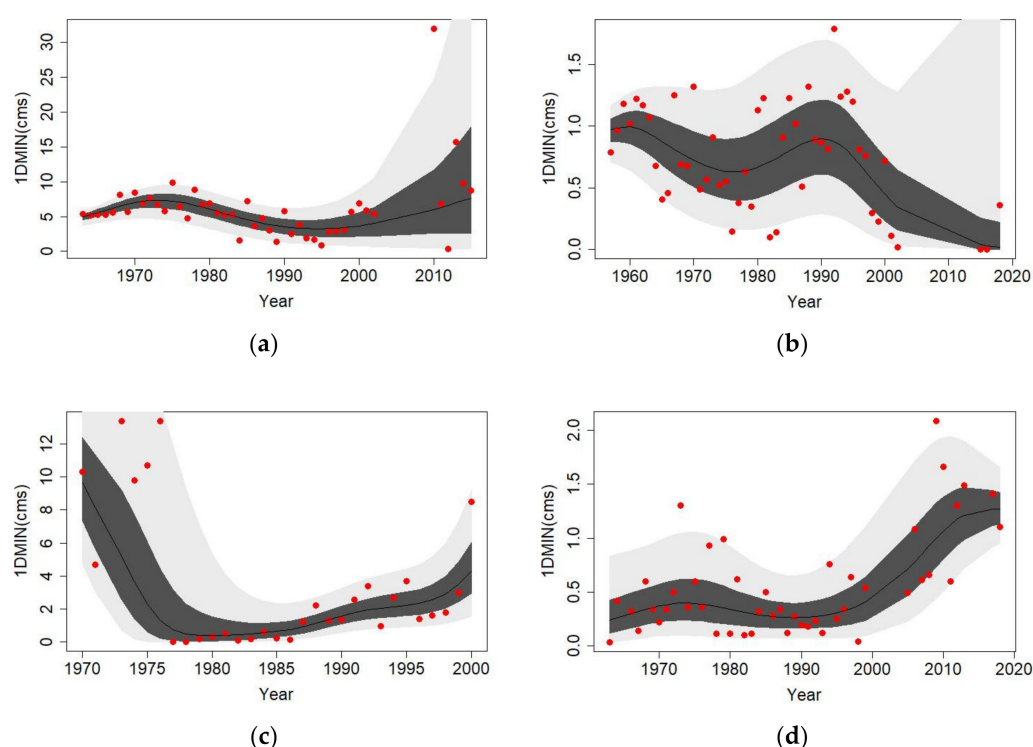
Figure 5. Variations of quantile curves (0.95, 0.75, 0.5, 0.25, and 0.05 from top to bottom) of 1DMIN (annual minimum 1-day streamflow) at (**a**) H2 (Xiayun), (**b**) H3 (Sanxia), (**c**) H5 (Xiulang), and (**d**) H7 (Wudu).

Table 7. Definition of the 16-category distributional changes and the corresponding number of flow indices belonging to each category.

		Variation in Variance			
		Increasing	No-Change	Decreasing	Complex Variation
Variation in mean	Increasing	I (4)	II (3)	III (0)	IV (1)
	No-change	V (2)	VI (4)	VII (1)	VIII (2)
	Decreasing	IX (0)	X (0)	XI (4)	XII (0)
	Complex variation	XIII (2)	XIV (0)	XV (0)	XVI (12)

Stationarity is not significant in the Tamsui River basin since only four indices (11.4%) are classified as Category VI (time-invariant mean and variance). The most prevalent category is XVI (complex variations of mean and variance), which has 12 indices and occupies 34.3% of all indices. The other indices are classified as Categories I, II, IV, V, VI, VII, VIII, XI, and XIII. Diverse categories of flow indices implies that no consistent streamflow alterations are observed in the Tamsui River basin. However, distributional changes between the maximum and minimum flow indices are different. The maximum inflow indices are classified only in Categories V, VI, VIII, XI, and XIII, where Categories VI, VIII, and XVI occupy 78.6%. Distributional changes of the minimum inflow indices are classified in 7 categories (I, II, IV, VII, XI, XIII, and XVI). The dominant categories include Categories XVI (42.9%), I (19.0%), and II (14.3%). Different distributional-change categories between the maximum and minimum flow indices reveal that different flow indices exhibit different alterations. For example, increasing mean does not exist in the minimum flow indices, and stationary mean and variance exist only in the maximum flow indices.

4.2. RI-Covariate Nonstationary Models of Maximum and Minimum Flow Indices

Effects of dams on streamflow regime alterations are evaluated in terms of the reservoir index, which is used as the covariate in the models of the maximum and minimum flow indices for various time scales. Table 8 reports the best-fitted probability distributions of the maximum and minimum flow indices using the reservoir index as the covariate at H2, H5, and H7, since these stations are located downstream of dams.

Table 8. Results of GAMLSS using RI as covariate.

Index	Parameter	H2	H5	H7
1DMAX	Dist.	GA	WEI	GA
	θ_1	c	c	ri
	θ_2	c	ri	c
2DMAX	Dist.	GA	WEI	LNO
	θ_1	c	c	ri
	θ_2	c	ri	ri
1DMIN	Dist.	GA	LNO	GA
	θ_1	ri	ri	c
	θ_2	ri	ri	c
7DMIN	Dist.	LNO	GA	LNO
	θ_1	c	c	c
	θ_2	c	ri	c
30DMIN	Dist.	LNO	LNO	GA
	θ_1	c	c	c
	θ_2	c	ri	c

Note: c: constant; ri: linearly varying with RI.

The results indicate that stationary distributions (constant parameters with RI) are observed at H2 (1DMAX, 2DMAX, 7DMIN, and 30DMIN) and H7 (1DMIN, 7DMIN, and 30DMIN). Streamflow regime at H2 is influenced by D1 and D2, which are check dams used to counteract erosion. Since D1 and D2 are not used for regulating streamflow, the maximum and minimum flow indices at H2 are related less to RIs, although high RIs are noted at H2. Low RIs observed at H7 leads to the minimum flow indices at H7, independent of RIs. All the maximum and minimum flow indices at H5 depend on RI because there are seven upstream dams for the purpose of water supply and hydropower generation. Heavily regulating of the streamflow of upstream tributaries of H5 induces the highly altered streamflow regime at H5. That is, the distribution parameters of the maximum and minimum flow indices at H5 are related to RIs.

Figure 6a–d illustrate variations of quantile curves (0.95, 0.75, 0.5, 0.25, and 0.05 from top to bottom) of 1DMAX and 1DMIN at H5 and H7, respectively. The abrupt changes of various quantile curves are observed in 1987 at H5, which is induced by the construction of D7, with the maximum capacity in this basin.

4.3. Discussion

The results of time-covariate modelling indicate that the streamflow regime of the Tamsui River basin is characterized by non-stationarity, since 31 out of 35 flow indices are best-fitted by the probabilistic models with time-dependent parameters. This phenomenon is prevalent in the minimum flow indices due to 100% of the flow indices belonging to nonstationary condition. This fact reveals that the minimum streamflow regime in the Tamsui River basin is highly vulnerable to climate change and anthropogenic activities. However, the effects of damming on streamflow characteristics of downstream stations (H2, H5, and H7) in terms of RI are insignificant since approximately half the indices (46.7%) do not relate to RIs.
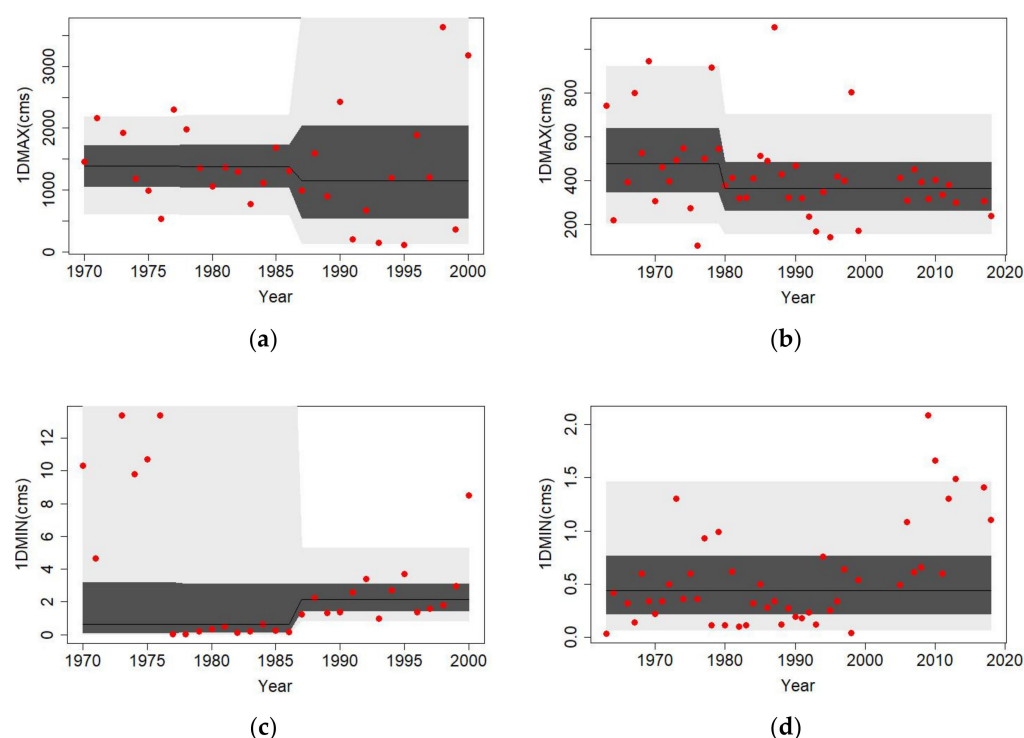
Figure 6. Variations of quantile curves (0.95, 0.75, 0.5, 0.25, and 0.05 from top to bottom) of 1DMAX (annual maximum 1-day streamflow) at (**a**) H5 (Xiulang) and (**b**) H7 (Wudu), and 1DMIN (annual minimum 1-day streamflow) at (**c**) H5 (Xiulang) and (**d**) H7 (Wudu).

Table 9 reports the AICs of the best-fitted distributions for the time-covariate and RI-covariate models. The lower-AIC model denotes the better model which is closer to the observed data. At H2, lower-AIC time-covariate models are observed in 2DMAX and all the minimum flow indices, except that an identical AIC is noted for the time-covariate and RI-covariate 1DMAXs, because both are fitted as stationary models. Lower-AICs RI-covariate models are observed in 1DMAX and 2DMAX and lower-AIC time-covariate models are observed in the minimum flow indices at H5. All the lower-AICs are noted for the time-covariate models at H7. The results indicate that the time-covariate models generally outperform the RI-covariate models.

Better time-covariate models are attributed to several factors. One of the reasons is that dams are not the most dominant factor in altering streamflow regime. Other anthropogenic factors including catchment development, population growth, and urban drainage, alter the streamflow regime. Besides, the low-RI such as 0.009 noted at H7 is also a factor leading to an insignificant covariate of RI. The purposes and operation of dams may cause different effects on streamflow changes. For instance, check dams such as D1 and D2 located upstream of H2 are used to reduce erosion, not to store and regulate streamflow, and have less effects on streamflow alterations. These factors, not involved in RI, make RI less related to streamflow alterations in Tamsui River basin.

Yeh et al. [39] indicated that the annual high flow ($Q_{0.9}$, daily discharge exceeded by 10% of days in a year) at H1 exhibited an insignificant increasing trend and an approximate null trend at H4 based on the Mann-Kendall test. Yeh et al. [39] also indicated that annual low flow ($Q_{0.1}$, daily discharge exceeded by 90% of days in a year) had insignificant decline and increasing trends at H1 and H4, respectively. Due to different definition and data length of flow indices, the results obtained by Yeh et al. [39] are not exactly identical to the results of this study, but parts of the results are consistent. For example, constant mean of 1DMAX at H4 and increasing mean of 1DMIN at H1 noted in this study are similar to the Mann-Kendall test results obtained by Yeh et al. [39]. Shiau and Wu [41] revealed that clearly increasing variance of the maximum 1-day rainfall is noted after 2000 at Taipei

station in the Tamsui River basin. This result is similar to the increasing variance observed at 1DMAX at H1, H4, and H5, but contradicts the decreasing variance of 1DMAX at H7. This fact implies that alterations in streamflow regime are not affected only by rainfall, but also by other complex factors such as watershed development, hydraulic-facility operation, the relationship between rainfall and streamflow, and others.

Table 9. Comparison of Akaike Information Criterion (AICs) for the time-covariate and Reservoir Index (RI)-covariate best-fitted models.

Index	Station	Time-Covariate	RI-Covariate
1DMAX	H2	744.60	744.60
	H5	478.72	**477.75**
	H7	**617.12**	624.26
2DMAX	H2	**709.21**	710.39
	H5	456.06	**455.39**
	H7	**594.85**	600.60
1DMIN	H2	**198.29**	237.73
	H5	**95.84**	111.85
	H7	**17.35**	39.02
7DMIN	H2	**198.44**	235.51
	H5	**120.31**	135.32
	H7	**32.42**	48.53
30DMIN	H2	**225.70**	249.64
	H5	**176.10**	184.60
	H7	**123.95**	125.58

Note: boldfaced numbers denote lower AIC.

The obtained nonstationary probability distributions of the flow indices offer more comprehensive information than the monotonic increasing or decreasing trends. For example, 1DMIN at H2 exhibits increasing mean and increasing variance (Category I and shown in Figure 5a), which is insufficiently described by increasing trend. However, the obtained best-fitted distributions are limited to the data periods used in the study; that is, the obtained time-varying models are not properly able to predict far-future streamflow conditions, indicated by Villarini et al. [51].

5. Conclusions

The main aim of this study is to explore non-stationarity of the maximum and minimum flow indices in terms of distributional changes for seven streamflow gauge stations in the Tamsui River located in northern Taiwan using the GAMLSS (generalized additive models for location, scale, and shape).

Results of time-covariate models indicate that stationarity is only noted in the maximum flow index, i.e., 1DMAX at H2, H3, and H6, and 2DMAX at H3. The streamflow regime in the tributaries (H3 and H6) is less influenced than those in the main rivers. Non-stationarity is prevalent in the minimum flow indices since all minimum flow indices are classified as nonstationary distributions. Clearly different distributional changes are observed among the flow indices. Streamflow regime in the Tamsui River generally exhibits non-stationarity because that 31 out of 35 (88.6%) flow indices have time-dependent distribution parameters. Category XVI (complex variations of mean and variance) is the dominant category since 34.3% of flow indices are classified in this category.

Results of RI-covariate models at H2, H5, and H7 indicate that constant parameters are observed at H2 (1DMAX, 2DMAX, 7DMIN, and 30DMIN) and H7 (1DMIN, 7DMIN, and 30DMIN). The reasons that these flow indices do not relate to RI are attributed to the dams located upstream of H2 used for counteracting erosion and the low RI (0.009) noted at H7. The RI-covariate models are generally worse than the time-covariate models. Only the RI-covariate 1DMAX and 2DMAX at H5 outperform the time-covariate models. This

fact indicates that construction of dams is not the only factor altering streamflow regime in the Tamsui River.

Based on the streamflow records used in this study, the results reveal that the streamflow regime in the Tamsui River is significantly altered except for 1DMAX and 2DMAX at some stations. Alterations in streamflow regime are attributed to climate change as well as to anthropogenic interferences. Prevalent non-stationarity in streamflow regime (88.6 % of flow indices) leads to approximate one third of flow indices (34.3%) exhibiting complex variation patterns instead of monotonic increasing or decreasing trends. RI is insufficient to describe dam-altered streamflow regime in the Tamsui River due to time-covariate modeling of 80% flow indices outperforming RI-covariate modeling. Complex anthropogenic interferences other than dam-construction need to be considered in the Tamsui River basin to evaluate spatially diverse alterations in streamflow regime.

Identification of non-stationarity in streamflow series gives an insight into streamflow regime alterations. This information can usefully guide future design and current operation of water-resources engineering, adapting to the changing environment. This study analyzes the non-stationarity in the maximum and minimum flow indices in the Tamsui River basin located in northern Taiwan. Construction of dams is not the unique factor influencing streamflow regime. Modification of the reservoir index to include purpose or operation types and other anthropogenic effects such as population or urban drainage remain as topics for further extending of this study.

Author Contributions: Conceptualization, J.-T.S.; methodology, J.-T.S.; software, Y.-T.L.; formal analysis, J.-T.S. and Y.-T.L.; data curation, Y.-T.L.; writing—original draft preparation, J.-T.S.; writing—review and editing, J.-T.S.; funding acquisition, J.-T.S. All authors have read and agreed to the published version of the manuscript.

Institutional Review Board Statement: Not applicable.

Informed Consent Statement: Not applicable.

Data Availability Statement: The streamflow data used in this study are provided from Water Resources Agency, Taiwan (https://www.wra.gov.tw (accessed on 5 March 2021)).

Conflicts of Interest: The authors declare no conflict of interest.

References

1. Salas, J.D.; Obeysekera, J. Revisiting the Concepts of Return Period and Risk for Nonstationary Hydrologic Extreme Events. *J. Hydrol. Eng.* **2014**, *19*, 554–568. [CrossRef]
2. Read, L.K.; Vogel, R.M. Reliability, return periods, and risk under nonstationarity. *Water Resour. Res.* **2015**, *51*, 6381–6398. [CrossRef]
3. Milly, P.C.D.; Betancourt, J.; Falkenmark, M.; Hirsch, R.M.; Kundzewicz, Z.W.; Lettenmaier, D.P.; Stouffer, R.J. Stationarity Is Dead: Whither Water Management? *Sci.* **2008**, *319*, 573–574. [CrossRef] [PubMed]
4. Cancelliere, A. Nonstationary Analysis of Extreme Events. *Water Resour. Manag.* **2017**, *31*, 3097–3110. [CrossRef]
5. Li, J.; Ma, Q.; Tian, Y.; Lei, Y.; Zhang, T.; Feng, P. Flood scaling under nonstationarity in Daqinghe River basin, China. *Nat. Hazards* **2019**, *98*, 675–696. [CrossRef]
6. Kalai, C.; Mondal, A.; Griffin, A.; Stewart, E. Comparison of Nonstationary Regional Flood Frequency Analysis Techniques Based on the Index-Flood Approach. *J. Hydrol. Eng.* **2020**, *25*, 06020003. [CrossRef]
7. Zhou, L.; Meng, Y.; Lu, C.; Yin, S.; Ren, D. A frequency-domain nonstationary multi-site rainfall generator for use in hydrological impact assessment. *J. Hydrol.* **2020**, *585*, 124770. [CrossRef]
8. Donat, M.G.; Lowry, A.L.; Alexander, L.V.; O'Gorman, P.A.; Maher, N. More extreme precipitation in the world's dry and wet regions. *Nat. Clim. Chang.* **2016**, *6*, 508–513. [CrossRef]
9. Prein, A.F.; Pendergrass, A.G. Can We Constrain Uncertainty in Hydrologic Cycle Projections? *Geophys. Res. Lett.* **2019**, *46*, 3911–3916. [CrossRef]

10. Markonis, Y.; Papalexiou, S.M.; Martinkova, M.; Hanel, M. Assessment of Water Cycle Intensification Over Land using a Multisource Global Gridded Precipitation DataSet. *J. Geophys. Res. Atmos.* **2019**, *124*, 11175–11187. [CrossRef]

11. Liu, B.; Tan, X.; Gan, T.Y.; Chen, X.; Lin, K.; Lu, M.; Liu, Z. Global atmospheric moisture transport associated with precipitation extremes: Mechanisms and climate change impacts. *Wiley Interdiscip. Rev. Water* **2020**, *7*, 1412. [CrossRef]

12. Tabari, H. Climate change impact on flood and extreme precipitation increases with water availability. *Sci. Rep.* **2020**, *10*, 13768. [CrossRef]

13. Konapala, G.; Mishra, A.K.; Wada, Y.; Mann, M.E. Climate change will affect global water availability through compounding changes in seasonal precipitation and evaporation. *Nat. Commun.* **2020**, *11*, 1–10. [CrossRef] [PubMed]

14. Dong, Q.; Wang, W.; Kunkel, K.E.; Shao, Q.; Xing, W.; Wei, J. Heterogeneous response of global precipitation concentration to global warming. *Int. J. Clim.* **2021**, *41*, 2347–2359. [CrossRef]

15. Gbode, I.E.; Ogunjobi, K.O.; Dudhia, J.; Ajayi, V.O.; Liu, C. Impacts of global warming on West African monsoon rainfall: Downscaling by pseudo global warming method. *Atmos. Res.* **2021**, *249*, 105334. [CrossRef]

16. Li, X.; Zhang, K.; Gu, P.; Feng, H.; Yin, Y.; Chen, W.; Cheng, B. Changes in precipitation extremes in the Yangtze River Basin during 1960–2019 and the association with global warming, ENSO, and local effects. *Sci. Total Environ.* **2021**, *760*, 144244. [CrossRef]

17. Ge, F.; Zhu, S.; Luo, H.; Zhi, X.; Wang, H. Future changes in precipitation extremes over Southeast Asia: insights from CMIP6 multi-model ensemble. *Environ. Res. Lett.* **2021**, *16*, 024013. [CrossRef]

18. Hirpa, F.A.; Alfieri, L.; Lees, T.; Peng, J.; Dyer, E.; Dadson, S.J. Streamflow response to climate change in the Greater Horn of Africa. *Clim. Chang.* **2019**, *156*, 341–363. [CrossRef]

19. Jahandideh-Tehrani, M.; Zhang, H.; Helfer, F.; Yu, Y. Review of climate change impacts on predicted river streamflow in tropical rivers. *Environ. Monit. Assess.* **2019**, *191*, 752. [CrossRef] [PubMed]

20. Kazemi, H.; Sarukkalige, R.; Badrzadeh, H. Evaluation of streamflow changes due to climate variation and human activities using the Budyko approach. *Environ. Earth Sci.* **2019**, *78*, 713. [CrossRef]

21. Li, S.; Zhang, L.; Du, Y.; Zhuang, Y.; Yan, C. Anthropogenic Impacts on Streamflow-Compensated Climate Change Effect in the Hanjiang River Basin, China. *J. Hydrol. Eng.* **2020**, *25*, 04019058. [CrossRef]

22. Gulakhmadov, A.; Chen, X.; Gulahmadov, N.; Liu, T.; Anjum, M.N.; Rizwan, M. Simulation of the Potential Impacts of Projected Climate Change on Streamflow in the Vakhsh River Basin in Central Asia under CMIP5 RCP Scenarios. *Water* **2020**, *12*, 1426. [CrossRef]

23. Sönmez, A.Y.; Kale, S. Climate change effects on annual streamflow of Filyos River (Turkey). *J. Water Clim. Chang.* **2020**, *11*, 420–433. [CrossRef]

24. Xiong, B.; Xiong, L.; Xia, J.; Xu, C.-Y.; Jiang, C.; Du, T. Assessing the impacts of reservoirs on downstream flood frequency by coupling the effect of scheduling-related multivariate rainfall with an indicator of reservoir effects. *Hydrol. Earth Syst. Sci.* **2019**, *23*, 4453–4470. [CrossRef]

25. Ray, L.K.; Goel, N.K. Flood Frequency Analysis of Narmada River Basin in India under Nonstationary Condition. *J. Hydrol. Eng.* **2019**, *24*, 05019018. [CrossRef]

26. Lu, F.; Song, X.; Xiao, W.; Zhu, K.; Xie, Z. Detecting the impact of climate and reservoirs on extreme floods using nonstationary frequency models. *Stoch. Environ. Res. Risk Assess.* **2020**, *34*, 169–182. [CrossRef]

27. Wang, Y.; Duan, L.; Liu, T.; Li, J.; Feng, P. A Non-stationary Standardized Streamflow Index for hydrological drought using climate and human-induced indices as covariates. *Sci. Total Environ.* **2020**, *699*, 134278. [CrossRef]

28. Osipova, N.V.; Bolgov, M.V. Assessing the Characteristics of the Maximal Spring Flood Runoff in the Don Basin under Nonstationary Conditions. *Water Resour.* **2020**, *47*, 945–952. [CrossRef]

29. Zhou, Y. Exploring multidecadal changes in climate and reservoir storage for assessing nonstationarity in flood peaks and risks worldwide by an integrated frequency analysis approach. *Water Res.* **2020**, *185*, 116265. [CrossRef] [PubMed]

30. Xiong, B.; Xiong, L.; Guo, S.; Xu, C.; Xia, J.; Zhong, Y.; Yang, H. Nonstationary Frequency Analysis of Censored Data: A Case Study of the Floods in the Yangtze River from 1470 to 2017. *Water Resour. Res.* **2020**, *56*, e2020WR027112. [CrossRef]

31. Yan, L.; Xiong, L.H.; Luan, Q.H.; Jiang, C.; Yu, K.X.; Xu, C.Y. On the applicability of the expected waiting time method in nonstationary flood design. *Water Resour. Manag.* **2020**, *34*, 2585–2601. [CrossRef]

32. Chu, P.-S.; Zhang, H.; Chang, H.-L.; Chen, T.-L.; Tofte, K. Trends in return levels of 24-hr precipitation extremes during the typhoon season in Taiwan. *Int. J. Clim.* **2018**, *38*, 5107–5124. [CrossRef]

33. Huang, W.-R.; Wang, S.-Y.S.; Guan, B.T. Decadal fluctuations in the western Pacific recorded by long precipitation records in Taiwan. *Clim. Dyn.* **2018**, *50*, 1597–1608. [CrossRef]

34. Kao, P.-K.; Hung, C.-W.; Hong, C.-C. Increasing influence of central Pacific El Niño on the inter-decadal variation of spring rainfall in northern Taiwan and southern China since 1980. *Atmos. Sci. Lett.* **2018**, *19*, e864. [CrossRef]

35. Wu, Y.; Wang, S.S.; Yu, Y.; Kung, C.; Wang, A.; Los, S.A.; Huang, W. Climatology and change of extreme precipitation events in Taiwan based on weather types. *Int. J. Clim.* **2019**, *39*, 5351–5366. [CrossRef]

36. Shiau, J.-T.; Chiu, Y.-F. Wavelet-Based Detection of Time-Frequency Changes for Monthly Rainfall and SPI Series in Taiwan. *Asia-Pac. J. Atmos. Sci.* **2019**, *55*, 657–667. [CrossRef]

37. Li, C.-Y.; Lin, S.-S.; Chuang, C.-M.; Hu, Y.-L. Assessing future rainfall uncertainties of climate change in Taiwan with a bootstrapped neural network-based downscaling model. *Water Environ. J.* **2020**, *34*, 77–92. [CrossRef]

38. Tung, Y.; Wang, S.S.; Chu, J.; Wu, C.; Chen, Y.; Cheng, C.; Lin, L. Projected increase of the East Asian summer monsoon (Meiyu) in Taiwan by climate models with variable performance. *Meteorol. Appl.* **2020**, *27*, e1886. [CrossRef]

39. Yeh, C.-F.; Wang, J.; Yeh, H.-F.; Lee, C.-H. Spatial and Temporal Streamflow Trends in Northern Taiwan. *Water* **2015**, *7*, 634–651. [CrossRef]

40. Rigby, R.A.; Stasinopoulos, D.M. Generalized additive models for location, scale and shape. *Appl. Stat.* **2005**, *54*, 507–554. [CrossRef]

41. Shiau, J.-T.; Wu, P.-S. Nonstationary Distributional Changes of Annual Rainfall Indices in Taiwan. *Asia-Pac. J. Atmos. Sci.* **2020**, 1–16. [CrossRef]

42. Khaliq, M.; Ouarda, T.; Ondo, J.-C.; Gachon, P.; Bobée, B. Frequency analysis of a sequence of dependent and/or non-stationary hydro-meteorological observations: A review. *J. Hydrol.* **2006**, *329*, 534–552. [CrossRef]

43. Yu, J.; Kim, T.-W.; Park, D.-H. Future Hydrological Drought Risk Assessment Based on Nonstationary Joint Drought Management Index. *Water* **2019**, *11*, 532. [CrossRef]

44. De Medeiros, E.S.; de Lima, R.R.; de Olinda, R.A.; Dantas, L.G.; dos Santos, C.A.C. Space-time kriging of precipitation: Modeling the large-scale variation with model GAMLSS. *Water* **2019**, *11*, 2368. [CrossRef]

45. Shiau, J.-T. Effects of Gamma-Distribution Variations on SPI-Based Stationary and Nonstationary Drought Analyses. *Water Resour. Manag.* **2020**, *34*, 2081–2095. [CrossRef]

46. Qu, C.; Li, J.; Yan, L.; Yan, P.; Cheng, F.; Lu, D. Non-Stationary Flood Frequency Analysis Using Cubic B-Spline-Based GAMLSS Model. *Water* **2020**, *12*, 1867. [CrossRef]

47. Stasinopoulos, D.M.; Rigby, R.A. Generalized additive models for location scale and shape (GAMLSS) in R. *J. Stat. Softw.* **2007**, *23*, 1–46. [CrossRef]

48. Lopez, J.J.; Frances, F.C. Non-stationary flood frequency analysis in continental Spanish rivers, using climate and reservoir indices as external covariates. *Hydrol. Earth Syst. Sci.* **2013**, *17*, 3189–3203. [CrossRef]

49. Li, J.; Tan, S. Nonstationary Flood Frequency Analysis for Annual Flood Peak Series, Adopting Climate Indices and Check Dam Index as Covariates. *Water Resour. Manag.* **2015**, *29*, 5533–5550. [CrossRef]

50. Jiang, C.; Xiong, L.; Xu, C.-Y.; Guo, S. Bivariate frequency analysis of nonstationary low-flow series based on the time-varying copula. *Hydrol. Process.* **2015**, *29*, 1521–1534. [CrossRef]

51. Villarini, G.; Smith, J.A.; Serinaldi, F.; Bales, J.; Bates, P.D.; Krajewski, W.T. Flood frequency analysis for the nonstationary annual peak records in an urban drainage basin. *Adv. Water Resour.* **2009**, *32*, 1255–1266. [CrossRef]